Effect of bed roughness on tsunami bore propagation and overtopping

Esteban, Miguel; Roubos, Jochem Jan; Iimura, Kotaro; Salet, Jorrit Thomas; Hofland, Bas; Bricker, Jeremy; Ishii, Hidenori; Hamano, Go; Takabatake, Tomoyuki; Shibayama, Tomoya
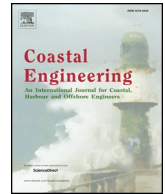
Important note
To cite this publication, please use the final published version (if applicable).
Please check the document version above.

Effect of bed roughness on tsunami bore propagation and overtopping

Miguel Esteban[a,*], Jochem Jan Roubos[b], Kotaro Iimura[a], Jorrit Thomas Salet[b], Bas Hofland[b], Jeremy Bricker[b], Hidenori Ishii[a], Go Hamano[a], Tomoyuki Takabatake[a], Tomoya Shibayama[a]

[a] Dept. of Civil and Environmental Engineering, Waseda University, 3-4-1 Ookubo, Tokyo, 169-8555, Japan
[b] Dept. of Hydraulic Engineering, Faculty of Civil Engineering and Geosciences, Delft University of Technology, Stevinweg 1, 2628CN, Delft, Netherlands

ARTICLE INFO

ABSTRACT

The accurate modelling of overtopping of coastal defences by tsunami waves is of vital importance for the formulation of disaster management strategies. To improve knowledge of this phenomena the authors conducted experiments on coastal structure overtopping using bores that were generated by a dam-break mechanism. Three types of structures were tested, namely a coastal dyke, a wall, and a wall of infinite height. The results highlight the necessity to consider the energy present in a bore to determine if a structure will be overtopped or not. As a result of these experiments an empirical formula to determine the height of overtopping given the incident bore height and velocity was validated. The study highlights the importance of clearly modelling the velocity and Froude number of a tsunami. Such experiments should be conducted on rough beds, for which a suitable Manning's n seems to be around 0.06 sm$^{-1/3}$. The study also contrasted the results obtained to those of the ASCE7 method, and concludes that the Manning's n values recommended in ASCE7 are probably too low.

1. Introduction

Tsunamis can devastate large portions of the coastline, inflicting severe casualties to any community situated on it that is not adequately prepared. To counteract these events, concrete structures have been built along large sections of coastlines at risk, particularly in the case of Japan. Despite the presence of such structures, the *2011 Tohoku Earthquake and Tsunami* (which generated run-ups of 10–40 m along the Tohoku coastline, Mori et al., 2012), went on to inflict casualties that sometimes exceeded 10% of the resident population (Yamao et al., 2015). Almost 20,000 people lost their lives in total, between those dead and still missing (The Japan Times, March 8, 2016), and 169 bn USD of assets were lost (equivalent to approximately 3% of the country's GDP (Ranghieri and Ishiwatari, 2014).

The failure of what was considered at the time a modern countermeasure system (Mori et al., 2012) has led to a re-assessment of the role of "hard" structures in tsunami disaster mitigation. Particularly, engineers have been trying to draw lessons about why some structures were overtopped but others were not. In areas where a bore might not have possessed enough energy only minor flooding was recorded behind the structures, such as in the case of Fudai. In this town floodgates and dykes were effective at dissipating the tsunami's energy, even though the structure was eventually partly overtopped (Fig. 1, left). However, throughout most of the coastline the defences were not high

enough, and the wave carried enough energy to overtop and destroy the town behind them (such as at Taro, for example, Fig. 1, right).

Following the 2011 event the Japanese coastal engineering community has started to classify tsunamis into two different levels, depending on their severity and intensity (Shibayama et al., 2013). Level 1 events would have a return period of several decades to around 100 years, and would result in smaller inundation heights than Level 2 events. Level 2 events would have return periods of a few hundred to a few thousand years, and for the case of substantial parts of the Japanese coastline would have inundation heights in excess of 10 m (Shibayama et al., 2013). The *2011 Tohoku Earthquake and Tsunami* is considered a Level 2 event, given that it has a return period greater than 1 in 1 000 years, though the tsunami height levels are calculated at each point of the coastline according to historical data on tsunami return periods. While there is some uncertainty on these, this change in philosophy essentially represents a move by Japanese disaster risk management to move to a probabilistic management of tsunami risk.

The determination of the tsunami level is crucial when it comes to the design of tsunami countermeasures. "Hard measures", such as breakwaters or coastal protection dykes, should be sufficiently high to protect residents and their property in the case of a Level 1 event. For the case of Level 2 events it is accepted that coastal defences would be overtopped, and that residents would have to rely on "soft measures", such as evacuation to higher ground or tsunami shelters. However, even

---

Fig. 1. Left: The dyke and floodgates at Fudai successfully stopped the tsunami, despite suffering some overtopping (inundation marks of ~20 m in front of the structure, indicated by the blue sign on the rightmost tower). Right: At Taro the massive coastal walls were overtopped, and the town behind them completely destroyed (pictures by authors). (For interpretation of the references to colour in this figure legend, the reader is referred to the Web version of this article.)

in this case hard measures are expected to survive the event, and should play a secondary role in slowing the advance of the tsunami and providing residents with extra time to evacuate (Tomita et al., 2012). For example, in the case of Otsuchi town, in Iwate prefecture, prior to the 2011 event the highest tsunami walls were built up to a height of +6.4 m T.P..[1] Simulations carried out by the national and prefectural governments indicate that the 1896 *Meiji-Sanriku* tsunami should become the benchmark for a Level 1 event (which required tsunami walls to be a level of +10.5 m T.P.) (Iwate Prefecture Tsunami Disaster Prevention Technical Committee, 2013). However, as the town is located close to Kamaishi city it was decided that most of the tsunami walls would be built to the same inundation height as that expected in Kamaishi, i.e. to a level of +14.5 m T.P (see Fig. 2, top left). Simulations indicate that even for such a wall partial overtopping is possible, allowing some water to flood the land behind it (Esteban et al., 2015). While the land behind the dykes has also been raised (Fig. 2, top right), it is necessary to understand to what extent the new dyke will be successful at stopping inundation behind it. Other similar dykes are being rebuilt elsewhere along the coastline (see Fig. 2, bottom).

In the aftermath of the 2011 event many field survey reports have analysed the types of failure mechanisms of coastal structures (Kato et al., 2012; Mikami et al., 2012; Mori et al., 2012; Jayaratne et al., 2016; Esteban et al., 2014). It is evident that beach bathymetry, coastal geomorphology, onshore coastal topography, coastal structure geometry and tsunami wave conditions, influence the failure modes and mechanisms of coastal structures (Kato et al., 2012; Mikami et al., 2014; Jayaratne et al., 2016). For the case of dykes, a number of authors (Kato et al., 2012; Mikami et al., 2014; Jayaratne et al., 2016) identified how leeward toe scour was the leading failure mechanism, though a number of other types of mechanisms could also be observed (Bricker et al., 2012; Kato et al., 2012; Tonkin et al., 2014; Jayaratne et al., 2016). Essentially, most structures were insufficiently strong to withstand the lateral and overtopping pressures and forces exerted on them, as they were based on research on solitary waves that had mostly not contemplated overtopping (see Tanimoto et al., 1984; Ikeno et al., 2001, 2003; Mizutani and Imamura, 2000; Esteban et al., 2009, 2012a, 2012b). However, following the 2011 event the use of solitary waves in tsunami modelling has been questioned, due to the relatively short distance between the source region and coast, compared to the distance in which a soliton forms (Madsen et al., 2008). Due to this, many researchers nowadays accept that the use of solitary waves can only be considered to reproduce the first stage of a tsunami wave as it reached the coastline (Goseberg et al., 2013). Hence, in recent times other

researchers have focused on the current velocity and overtopping effects to design armour of breakwaters against tsunami attack (Sakakiyama, 2012; Hanzawa et al., 2012; Kato et al., 2012), even though it is difficult to accurately replicate such effects in the lab.

It is important to note how, despite failing, protection structures might have played a role in mitigating tsunami damage (Nateghi et al., 2016), as highlighted by field surveys (Mikami et al., 2012; Suppasri et al., 2012; EERI, 2011; Omira et al., 2013; Latcharote et al., 2016) and numerical simulations (Nandasena et al., 2012; Stansby et al., 2008; Hunt-Raby et al., 2011). One of the more significant of such structures was the Kamaishi tsunami breakwater, the deepest breakwater built anywhere in the world. Following the disaster, Tomita et al. (2012) conducted simulations that show that the structure could have reduced inundation heights in Kamaishi city from 13.7 m to 8.0 m, providing residents an extra 6 min to evacuate (though the effect of the damaged sections of this breakwater was neglected in the calculations of tsunami approach time, Cyranoski, 2012). However, other more typical breakwaters were basically designed to reflect wind waves, and the reduction of the tsunami impact due to them should also not be overestimated (Takagi and Bricker, 2014).

Thus, the 2011 event triggered an abundance of research dealing with the stability of tsunami countermeasures, though comparatively little experimental research has been conducted on understanding the overtopping of tsunami-induced flows over tsunami walls or dykes. To properly understand the benefits of coastal structures that are overtopped, as is expected for Level 1 tsunamis, it is important to determine the volume of water, flooding depth (d_f) and velocity (v) that can result from an overtopping tsunami. The $d_f\,v$ product is particularly important, as values higher than $0.5\,m^2/s$ can result in 50% mortality, which increases to almost 100% when $d_f\,v\,>\,2\,m^2/s$ (Jonkman and Penning-Rowsell, 2008). If correctly designed, these structures can play a critical role in lowering this $d_f\,v$ value, and provide residents with extra time to evacuate (Okumura et al., 2017; Takabatake et al., 2017, 2018). Coupled with improved evacuation procedures and communication, such disaster management systems would make it easier for residents and visitors to an area evacuate in the case of a tsunami (San Carlos-Arce et al., 2017).

As a result, Esteban et al. (2017) set out to investigate overtopping flow patterns that result from a variety of different incident bore-type conditions. The laboratory experiments detailed by these authors were then followed by detailed computer simulations by Glasbergen (2018), using a bathymetry that attempted to simulate typical beach profiles along the Sendai planes, in the northern Tohoku region in Japan. The results of Esteban et al. (2017) and Glasbergen (2018) showed that whether a structure is overtopped or not will depend on the energy in the bore, with lower velocity bores less likely to overtop a structure than higher velocity ones.

---

[1] These heights are presented relative to Tokyo Peil (T.P. corresponds to mean sea level of Tokyo Bay).

Fig. 2. Top left. Construction of new dyke in Otsuchi town (Sept 2018). Top right. New park in Otsuchi, showing the original level of the town (pond on the right) and the new level (houses at the back). Bottom left. Reconstructed dike along the Sendai plains coastline (photo courtesy of Glasbergen, T). Bottom right. New coastal dyke at Rikuzentakata, in front of a preserved memorial building.

However, the experiments of Esteban et al. (2017) suffered from the limitation of only having been carried out on a smooth bed, and thus did not take into account the effect of different (and more realistic) bed roughness coefficients. Furthermore, it is not clear whether the high velocities and Froude numbers obtained using a dry bed are truly representative of a tsunami-like flow. Thus, in the present work the authors set out to address this problem by conducting a new set of experiments on a rough bed, which were then compared to the original results detailed in Esteban et al. (2017). The authors then provide some guidelines as to how high a structure would have to be so that it can effectively help in the evacuation of citizens against a Level 2 tsunami.

However, tsunamis can also represent a threat to coastal communities outside Japan. The ASCE7 (ASCE, 2016) became the first North American standard that is written in mandatory language, addressing tsunami hazards and how these apply to the context of North America (Stolle et al., 2019). The International Building Code (IBC) references design provisions that are provided for in the ASCE7 Standard, and thus has become part of an enacted building code law through adoption of the model International Building Code by the state, county, or city (Chock, 2015). This guideline contains a simplified method (called the Energy Grade Line, or EGL, method) to establish maximum tsunami inundation depth and flow speed values, based on inundation maps throughout the United States. The present research will also attempt to validate the accuracy of such a model, in light of the laboratory experiments carried out in the present work, and the simulations conducted by Glasbergen (2018).

2. Experimental program

Two different rounds of laboratory experiments (in Sept 2017 and Sept-Oct 2018) using a dam break generation mechanism were performed in a wave flume (dimensions $14\,m \times 0.41\,m \times 0.6\,m$) at Waseda University, Tokyo, Japan. The first analyses of the 2017 smooth-bed tests was given by Esteban et al. (2017). Froude scaling of 1:50 was used when converting the velocity of the bore to real-life

conditions, to see how accurately the wave resembled that of a real life tsunami event. A schematic representation of the wave tank and the apparatus in it, as used for both tests series, is shown in Fig. 3. On the left side of the tank a dam break generation mechanism was operated by a system of pulleys attached to a heavy weight (See Fig. 4). The opening height of the gate was 15 cm. As the weight was not changed throughout the experiments, the gate opening speed also remained constant. Behind this gate a 4.5 m reservoir ensured that there was enough water to generate a long bore (water levels behind the gate varied between experimental cases, meaning that between 18.9 and $37.8\,m^3$ of water was released each time). In total, 12 experimental cases were carried out, for water levels in the reservoir of $d = 30, 40, 50$ and 60 cm, and water levels in front of the reservoir of $h = 0, 10$ and 20 cm.

A metal false bed was constructed on top of the floor of the tank, with the start of the sloping section being only 5 cm away from the edge of the gate. The horizontal section of the false bed was 20 cm above flume bed, with the slope of the initial section being 1:10. All of the experimental cases were repeated for two false bed conditions. The first was the smooth metal finish of the actual bed. For the second condition, acrylic layers were fixed on top of the false bed, with small diameter stones (3–5 mm, corresponding to a Manning $n = 0.02\,sm^{-1/3}$ according to Limerinos, 1970) being glued to the entire face of each of the panels. This made the bed in the rough bed case slightly (ca. 5 mm) higher. Note that there are more physically realistic ways than Manning's n to parameterize bed roughness (see for example the discussion at the end of Bricker et al., 2015), but Manning's n still pervades the practice of inundation modelling and is encoded by the ASCE7, so it is thus the focus of the present study.

The test section was located 1.65 m away from the top end of the sloping part of the false bottom, with three different structures being tested: (1) a coastal dyke, (2) a low tsunami wall and (3) a high tsunami wall (this wall was not overtopped, so it can be regarded as a wall of "infinite height"). The dyke was constructed using a combination of acrylic panels and a hollow metallic structure (9.5 cm high, 26 cm long
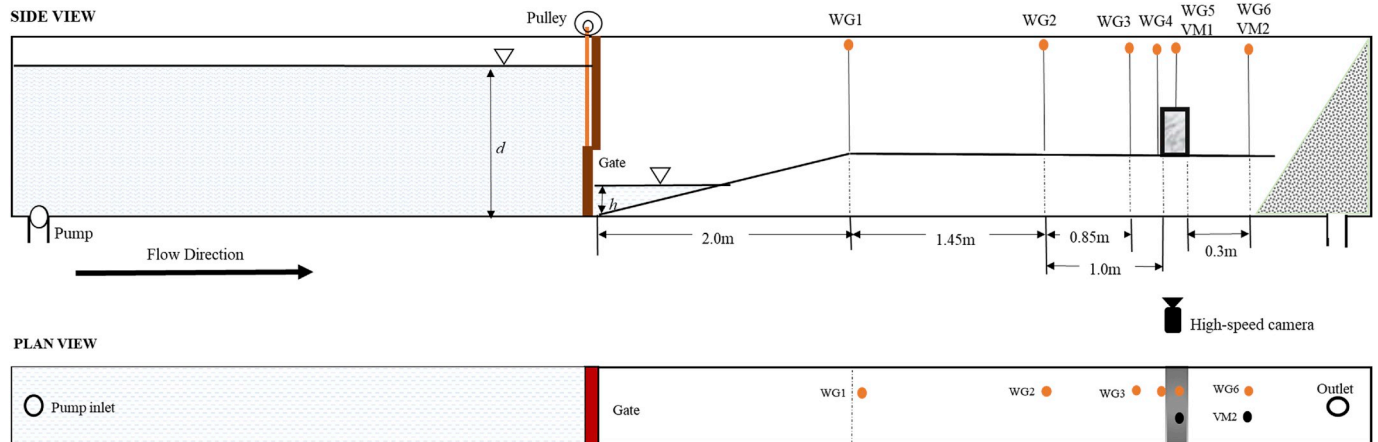
Fig. 3. Schematic of the wave flume and intrumentation [not to scale].

Fig. 4. Experimental Apparatus. a) View of the back of the gate. b) Weight system to release the gate. c) Wave gauge and velocity meters (smooth flat bed). d) Stone flat bed.

across the base and 6 cm wide at the top, see Fig. 5). The low tsunami wall was essentially one concrete block 15 cm high and 10 cm wide (Fig. 5). The high tsunami wall consisted of a 39 cm high acrylic panel, supported at the base by a concrete brick (Fig. 5). The false bed and all of the test structures were fixed to the sides of the wave tank using silicon, and particular attention was paid to them being completely sealed. No movement was observed in any of the structures or false bed during the experiments. At the end of the tank a wave absorption beach was constructed, under which there was a drain that allowed for excess water to be removed after each experiment.

Several wave gauges (WG) and velocity meters (VM) were placed in the tank, as shown in Fig. 1. All gauges (KENEK CHT6–30, 40) were of the capacitance type, with a range of either 30 or 40 cm. Table 1 shows a summary of the experimental conditions (note that some definitions in the table will be further elaborated in the section detailing the results). To evaluate the hydrodynamic conditions of the waves that were generated experiments were also performed without any structures being present inside the tank, focusing on the unobstructed water surface elevation and velocity profile just before the test area. The instruments used a data logging system (KENEK ADS2016), which was connected to a PC. The sampling frequency of all measurements was 200 Hz. A high-speed Nikon D5200 camera (60 frames per second) was mounted on a tripod directly in front of the structures. This allowed the analysis of the profile of the bores as they hit the structures, and the overflowing patterns that resulted from them.

The velocity meters (KENEK VMT2–200–04P, 04 PL) used in the experiment were all electromagnetic current meters (ECMs), with a range of measurement of 2 m/s. A low pass filter of 20 Hz was applied after the data acquisition. They were placed at the top of the structure

and 15 cm behind it, to attempt to measure the overtopping conditions. However, due to air bubbles entrained within the turbulent bore and disturbance of the free surface due to the high-speed flow around the probe head, the complete velocity profile could not be accurately recorded for the entire length of the experiments. Thus, the measurements obtained by this type of instrumentation were considered to be approximate reference values, and the bore front velocities were measured from the wave gauge (WG) data, as will be discussed later.

In preparation for each of the experimental cases the tank was drained and filled to the specified height with water (both for the case of the water in the reservoir and that in the main test section). It should be noted that wet bed conditions were used in all experimental conditions. To ensure replicability certain experimental conditions were repeated five times, as will be discussed later in this paper.

$T/2$ (the "wave half-period" of the "tsunami-like wave") was estimated from the wave profile of the experimental cases where no structure was present in the tank. For the experimental cases with less water, $T/2$ could be calculated precisely (For example, for the smooth bed experiments $T/2 = 10.6$ s for $d = 30$ cm and $h = 0$ cm, which would correspond to a real life $T/2 = 74.9$ s) However, as the amount of water in the reservoir was increased the wave was faster and it reached the end of the tank and was reflected before a full cycle could be recorded. Thus, it was only possible to conclude that, $T/2 > 16.1$ for $d = 60$ cm and $h = 0$ cm for the smooth bed (corresponding to a real life tsunami $T/2 > 113.8$ s). For the case of the rough bed, the wave appeared to advance slower, and for $d = 30$ cm a secondary wave (reflected from the sloped section onto the gate and back onto the structure) reached the test section before a full cycle was finished. Thus, it was only possible to conclude that $T/2 > 12.18$ s for $d = 30$ cm and
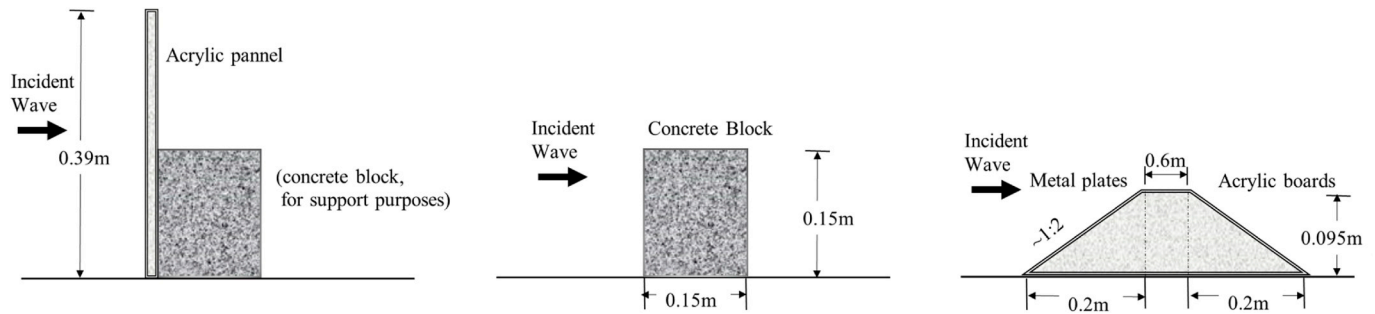
Fig. 5. The structure types tested [not to scale]. From left to right, "high vertical wall", "low vertical wall" and dyke.

$h = 0$ cm and $T/2 > 14.12$ s for $d = 60$ cm and $h = 0$ cm for the rough bed (real life $T/2$ of 86.1 and 99.8 s, respectively). Despite this limitation, a $T/2 > 10$ s meant that the experiments were able to reach a quasi-stationary overtopping flow (for the experimental cases where overtopping took place), which could be considered similar to what was observed during the *2011 Tohoku Earthquake and Tsunami*.

3. Results

3.1. Experiment repeatability

When performing tests using dam-break experiments it is important to ascertain whether these are consistent. Esteban et al. (2017) proved this by repeating experiments 5 times for the case of the "low tsunami wall" and "dyke" structure experiments with $d = 50$ cm and $h = 0$ cm (showed in bold italics in Table 1). For the case of the rough bed the coefficient of variation from the averaged maximum water level recorded at each gauge was low, as shown in Table 2.

However, the measurements by the velocity metres were much less consistent, for both the rough and smooth bed conditions. In this sense,

Table 2
Summary of the coefficient of variation for the various experiments conditions, for $d = 50$ cm and $h = 0$ cm (based on 5 experiments).

Structure	Bed type	WG1	WG3	WG5	WG6
Low Vertical Wall	Smooth bed	1.2%	1.9%	13.5%	10.6%
	Rough bed	3.8%	0.6%	12.0%	6.3%
Dyke	Smooth bed	1.2%	1.7%	4.8%	6.3%
	Rough bed	1.0%	4.2%	6.9%	5.3%

the present experiments were unable to improve on the methodology of Esteban et al. (2017) and were thus omitted (the velocity meters are electromagnetic instruments that do not produce reliable results in conditions of substantial air entrainment).

3.2. Dam break wave profile

As stated earlier it was difficult to get accurate readings from the velocity metres, as the velocity of the incident bores typically exceeded their capabilities (full range of 2 m/s), and the entrapment of air behind
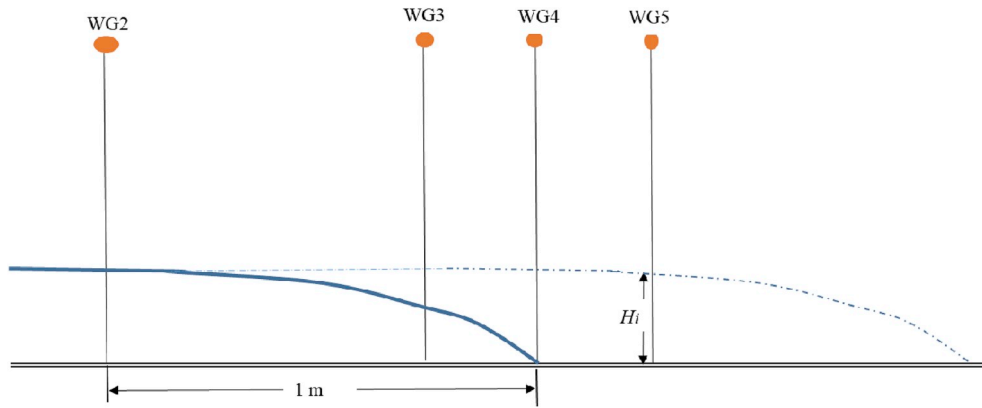
Table 1
Summary of experimental conditions and results (note that some of the variables mentioned will be defined in the section detailing the results). Numbers in bold italics indicate the experimental conditions ($d = 50$, $h = 0$ cm, for both the low vertical wall and the dyke) that were repeated 5 times. Results for the smooth bed case are repeated from Esteban et al. (2017).

Rough Bed	Water depth in reservoir/in front of the reservoir		Structure Type								
			No structure		High vertical wall (non-overtopped)	Low vertical wall			Dyke		
No	d [cm]	h [cm]	Hi [cm] WG5	Vi [m/s] WG2-4	$Hf0$ [cm] WG3	Hf [cm] WG3	Ho [cm] WG5	Hb [cm] WG6	Hf [cm] WG3	Ho [cm] WG5	Hb [cm] WG6
	30	0	3.42	1.24	8.24	8.57	0	0	8.06	0.41	1.43
		10	3.67	1.15	7.79	7.15	0	0.02	8.57	0	0.61
		20	3.73	0.88	8.2	7.49	0	0.02	8.7	0.04	0.12
	40	0	5.49	1.68	16.15	15.21	0.9	1.48	13.73	5.55	4
		10	5.64	1.37	14.59	14.46	0.21	1.41	13.39	4.41	2.4
		20	5.64	1.79	15.41	14.85	0.57	1.62	13.58	3.89	2.58
	50	0	8.59	2.12	24.3	*21.04*	*10.76*	*5.31*	*17.61*	*11.35*	*7.56*
		10	7.79	1.92	22.38	19.28	4.92	3.26	17.11	9.22	6.88
		20	8.32	1.66	21.41	20.16	5.31	4.3	17.97	10.45	7.38
	60	0	12.17	2.59	33.69	27.55	16.33	9.45	20.32	16	9.92
		10	10.74	2.43	28.61	24.35	11.11	6.95	20.36	13.16	8.95
		20	10.27	2.7	28.63	24.17	12.38	6.88	20.89	13.48	10.12
Yes	30	0	3.38	0.99	8.59	8.81	0.03	0.04	7.62	0	0
		10	3.11	0.86	7.44	6.89	0	0	7.48	0	0
		20	3.28	0.78	8.32	7.38	0.03	0.04	8.01	0	0
	40	0	5.63	1.36	18.13	16.07	0.32	0.62	15.27	5.19	2.61
		10	5.23	1.28	16.46	14.18	0.28	0.03	13.87	2.99	2.02
		20	5.86	1.29	17.66	16.13	0.72	1.99	13.85	3.22	2.21
	50	0	7.95	1.82	25.98	*21.59*	*6.518*	*3.784*	*19.138*	*9.234*	*4.844*
		10	7.5	1.49	24.08	22.54	4.1	3.69	18.09	7.22	4.2
		20	8.01	1.27	26.35	21.88	7.63	2.61	18.4	11.06	3.37
	60	0	10.55	1.96	33.55	28.38	12.29	7.15	24.34	13.67	8.13
		10	9.96	1.65	32.95	35.55	10.27	6.24	21.21	12.08	7.6
		20	10.76	1.42	32.38	31.45	11.65	4.66	21.43	12.38	6.09

Fig. 6. Diagramatic representation of the calculation of the bore velocity V_i. The continous line indicates the wave profile as the bore reaches WG4. H_i, the incident (unobstructed) wave height, was taken as the maximum water lever at WG5 (with the discontinous line showing the wave profile at this moment).

the probes resulted in missing data points (also reported in Esteban et al., 2017). To overcome this problem, the authors used the bore front velocity to approximate the maximum kinetic energy present in the wave-like flow (following Dressler, 1954; Estrade and Martinot, 1964; and Chanson, 2006, who estimated that the flow velocity in the turbulent bore tip is roughly equal to the bore front velocity). As the experiments were conducted over a horizontal, flat, unobstructed surface, the bore front velocity should represent the maximum velocity of the flow.

Following Esteban et al. (2017), the bore front velocity was thus calculated by measuring the time for the bore tip to travel between WG2 and WG4 (which were situated 1.0 m apart from each other) when no structure was present in the tank (see Fig. 6). The incident wave height (H_i) was considered to be the maximum height of the wave as it traversed WG5 (as this was the location of the centre of the structures in the other experimental cases), with Table 1 also showing the values of V_i. When no structures were present the bore appeared uniform as it made progress over the false bed (i.e. there appeared to be no change in its profile between WG4 and WG5, see Fig. 6). This obviously changed when the structres were placed inside the tank, as the wave crashed into the structure and overtopped it (if it had sufficient kinetic energy).

The notional Froude number Fr for the bore front given in Fig. 6 is defined by equation (1).

$$Fr = \frac{V_i}{\sqrt{gH_i}} \qquad (1)$$

It is important to remember that this Fr is not the steady flow Froude number, given that it is a front propagating over a dry bed, and that the front velocity and (maximum) flow depth are measured at different times. The Fr for the rough bed and smooth bed experiments was clearly different, as shown in Fig. 7. This indicates that the bore front slows down and steepens up due to the roughness. There are indications that the lower Froude numbers of the rough bed experiments are more realistic than those of the smooth bed, according to Glasbergen (2018) and Matsutomi et al. (2001). The SWASH simulations conducted by Glasbergen (2018) indicate that in the coastal area (around 300–500 m from the seashore) the Fr number for a tsunami-like propagating front should be in the order of 1. Matsutomi et al. (2001) summarized Froude numbers for past tsunami events, which they calcuated using the surveyed flow depths and velocities estimated from Bernoulli's equation, and showed that they ranged from 0.7 to 2.0 near the shoreline.

In order to get a more direct view of the change in bore shape due to the roughness, the slope of the wave front was measured from the video images that were recorded during the tests. The image taken at the moment that the front made first contact with the wall was used for the analysis. Then, the water depth of the wave at a distance of 30 cm from the wall was read from the image. The water surface could be
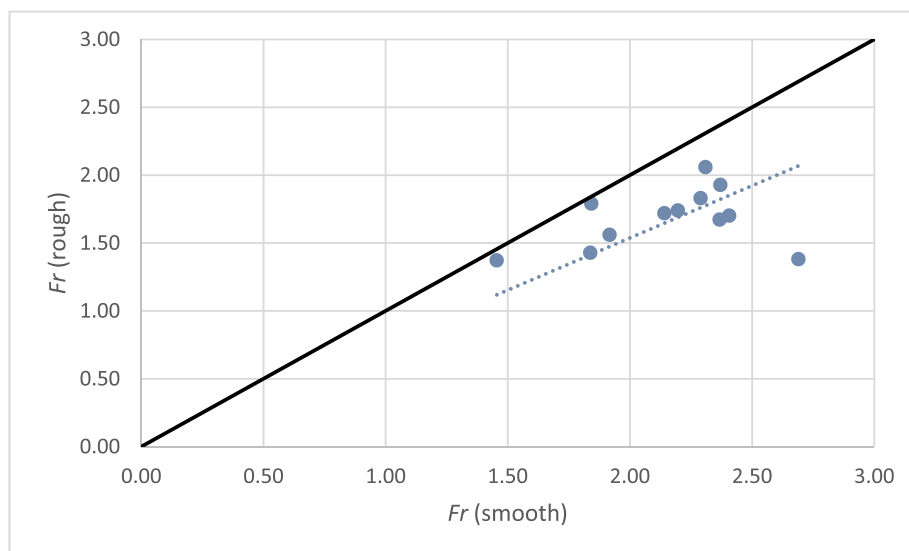

Fig. 7. Comparision of Fr numbers for the rough and smooth bed experimental conditions for the range of experimental conditions provided in Table 1.
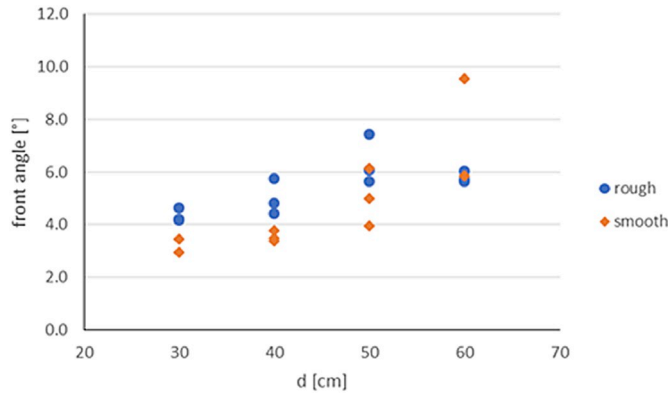
Fig. 8. Comparison of direct video measurement of front slope angle for smooth and rough beds, for different water depths (d) in the reservoir.

distinguished best by observing a series of pictures from the movie recording, with the image coordinates being transformed into real-life coordinates by relating the pixel size to objects of known size in the image (that were located at the same distance from the camera as the water surface). The pixel size ranged from 0.5 to 1 mm. No image correction was applied, so that the accuracy was estimated to be better than 5%. From Fig. 8 it can be seen that the front slope of the wave on the rough bed seems to be steeper than that on the smooth bed. The only cases in which this trend is not clear are for the tests with the largest initial water level ($d = 60$ cm).

3.3. Inundation height after the structure

Esteban et al. (2017) introduced a number of parameters to analyse the wave overtopping. H_f, H_o and H_b are the maximum values of the water surface elevation of the bore as it impacts, overtops and continues to run behind the structure (which were obtained from WG3, WG5 and WG6, respectively). These parameters are diagramatically explained in Fig. 9. All experiments showed a similar pattern, with the front rapidly approaching the structure and eventually overtopping it if it had enough kinetic energy. A quasi-stationary overtopping flow was subsequently achieved (with the durations indicated by $T/2$ earlier), which would last several minutes for the case of real tsunamis, though in the case of the laboratory water quickly ran out.

In basic wave hydraulics the energy of an incoming steady flow traversing WG5 without structure would be given by equation (2)

$$E_i = \frac{V_i^2}{2g} + H_i \tag{2}$$

where E_i is the total head, V_i is the flow velocity (for which we here take the maximum incident bore front velocity in front of the structure), g is the acceleration due to gravity, and H_i is the water level (for which we here take the maximum incident water level relative to the flume false

bottom, as defined in Fig. 4).

The authors first summarized the data for the high wall case (which was not overtopped and can hence be regarded as the maximum run-up), by using the maximum value recorded at WG3, placed close to the front of the high seawall, which is referred to as H_{fo}. It is assumed that H_{fo} is a stagnation pressure that is equal to the incoming 'energy head' E_i, which was also corroborated by Esteban et al. (2017). Fig. 10 shows the relationship between static head at the edge of the gate relative to the elevation of the false bottom ($d - 0.2$ m) and Ei, showing how the rough bed dissipates some of the energy of the incoming wave.

Esteban et al. (2017) provide a formula to estimate the inundation height after a structure of a given height H_w, given the total head of the incident front E_i (which can be calculated according to its incident wave front velocity V_i and wave height H_i). The ratio H_b/H_i is given by the relationship between the ratio of wave depth after the wall [H_b] to the incident wave height [H_i] and the E_i/H_w

$$H_b/H_i = \tanh\left(0.51\frac{E_i}{H_w} - 0.36\right) \qquad (R^2 = 0.89) \tag{3}$$

The formula is applicable for both dykes and vertical walls, for structures and tsunamis where $0.2 < H_i/H_w < 1.3$. In the present work the authors verified that the equation is still applicable for rough beds, and that its range of applicability is independent of the roughness of the bed or Froude number of the bore, as shown in Fig. 11.

3.4. Comparison of results with the ASCE 7 energy gradeline method

The ASCE7 (ASCE, 2016) contains a simplified method (called the Energy Grade Line, or EGL, method) to establish maximum tsunami inundation depth and flow speed values, based on inundation maps throughout the United States. As explained in detail in Kriebel et al. (2017), the EGL assumes that a conservative way to calculate the maximum inundation depth and flow speed values along a 1-dimensional transect normal to the shoreline is via the total head equation (2), starting at the point of maximum runup (known elevation and zero kinetic head), and calculating back towards the shoreline. Moving towards the shoreline, the friction loss is added back into the total head (4) via Manning's equation (5)

$$E_i = E_{i-1} + s_i\Delta x \tag{4}$$

$$s_i = \frac{u_i^2}{\left(\frac{1}{n}\right)^2 h_i^{\frac{4}{3}}} \tag{5}$$

where s is frictional head loss slope, E is total head, Δx is the distance between calculation points i and $i-1$, u_i is the maximum flow speed at point i, n is Manning's n, and h_i is maximum flow depth at point i.

The experiments of this paper provide a chance to check the Manning's n values suggested by ASCE7 for Equation (5) against physical results. To do this, a simple HEC-RAS version 5.0.6 unsteady flow model (Bruner, 2016), which uses the one-dimensional St. Venant
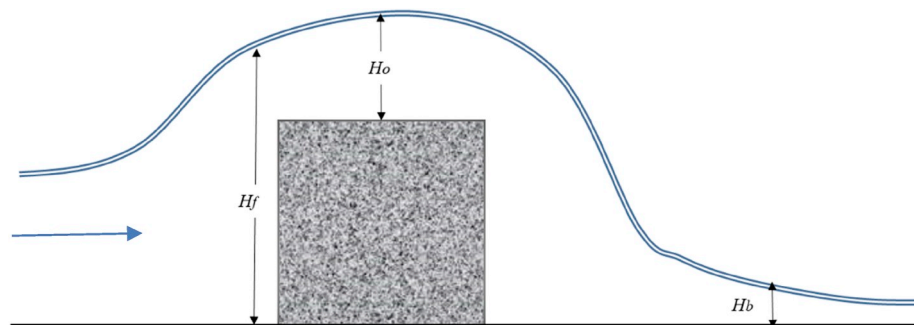

Fig. 9. Wave parameters used to analyse the overtopping wave. H_f, H_o and H_b represent maximum values of the surface profile of the wave as it impacts, overtops and runs past the wall. These values were obtained from WG3, WG5 and WG6, respectively.
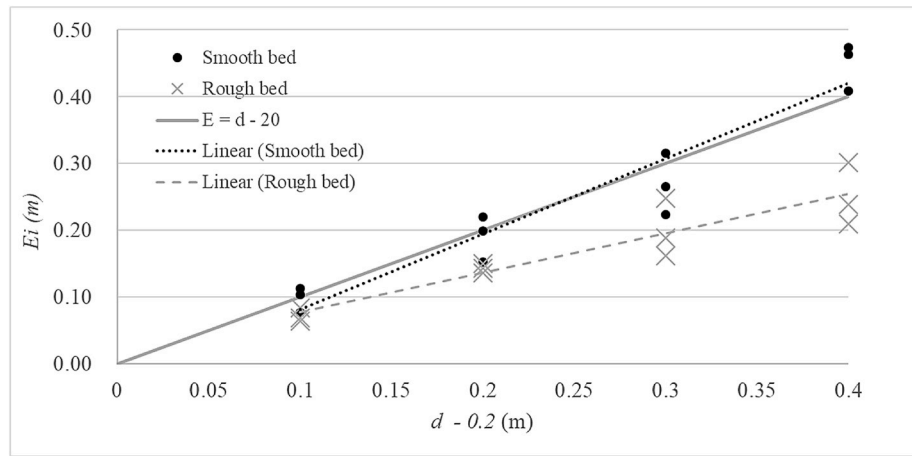
Fig. 10. Relationship between E_i and static head at the edge of the gate for the high seawall.
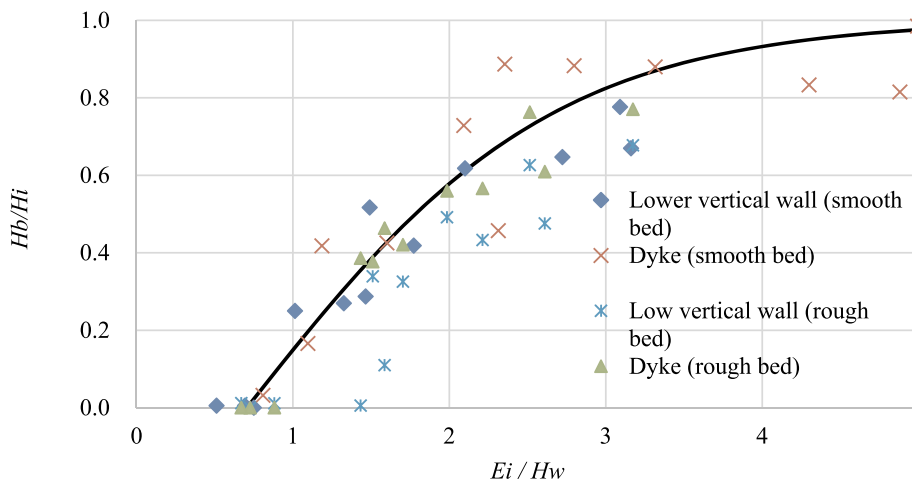

Fig. 11. Relationship between the ratio of wave depth after the wall [H_b] to the incident wave height [H_i] and the E_i/H_w.

equations, was implemented to estimate flow depths and speeds throughout the flume. HEC-RAS has been shown to model 1-dimensional dam breaks with enough accuracy for practical applications (Bricker et al., 2017). The model was set up to run with a cross-section spacing of 1 cm and a time step of 0.1 s. Initial conditions represented the water levels within and in front of the reservoir, and the gate was assumed to open instantaneously, with an orifice coefficient of 0.8. Since HEC-RAS assumes a rough bed, it was compared only to the rough bed experiments detailed earlier in this paper. Model calibration resulted in a Manning's $n = 0.03$ s/m$^{1/3}$ (model scale) best approximating the bore speed and depth at each wave gauge. Fig. 12 shows the comparison of water depth time series at each wave gauge.

The lesson from these laboratory experiments is related to the Manning's n values in Eq. (5), for which ASCE7 recommends values of 0.025 sm$^{-1/3}$ for "coastal water or nearshore bottom friction, or open land or fields", 0.04 sm$^{-1/3}$ for urban areas, and 0.03 sm$^{-1/3}$ for all other cases. For coastal and open areas, these suggested values are similar to those for steady flow (i.e., Chow, 1959), but for urban and vegetated areas, much larger values are suggested for both steady and unsteady flows (Bricker et al., 2015). The rough bed laboratory experiments presented in this resarch utilized stones 3–5 mm in diameter (d_{50} approximately 4 mm). Limerinos (1970) relates the median stone diameter d_{50} and the hydraulic radius R to Manning's n in steady flow via Eq. (6).

$$\frac{n}{R^{1/6}} = \frac{0.0926}{0.35 + 2.0 log_{10}\left(\frac{R}{d_{50}}\right)}$$

(6)

For the shallow, wide flume, the hydraulic radius is approximately equal to the flow depth, which for the bores shown in Fig. 12 is on the order of 0.05 m. The resulting Manning's n from Eq. (5), intended for steady flow, is 0.02 sm$^{-1/3}$. However, the calibrated HEC-RAS model required $n = 0.03$ sm$^{-1/3}$ to correctly capture the waveforms of Fig. 12, indicating that the steady-flow Manning's n value was too small for the unsteady dam-break flow of the experiments. Bricker et al. (2015) suggests that tsunamis require larger effective Manning's n values than steady flow because of the enhanced turbulent dissipation of energy in the unsteady flow bottom boundary layer (Bricker et al., 2005); Williams and Fuhrman (2016) and Larsen and Fuhrman (2019b) corroborate this further by showing the bottom boundary layer under a tsunami to be unsteady, therefore not reaching the full water depth. Since Manning's n scales with the geometric scale to a power of 1/6, the Manning's n value expected for a tsunami over this terrain at prototype scale (the bed grains themselves correspond to cobbles of 20 cm diameter at prototype scale) is $n = 0.06$ sm$^{-1/3}$, which is again much larger than any of the Manning's n values suggested by ASCE7 (ASCE 7 suggests a maximum value of $n = 0.04$ sm$^{-1/3}$, for "buildings of at least urban density", which are much larger than cobbles).

Since the suggested application of Eq. (4) and Eq. (5) in the EGL method is to begin at the location of runup (the edge of inundation) on a hazard map, and then to calculate total head E_i seaward up to the shoreline, the incremental friction head s_i (Eq. (5)) is added back into the total head at each spatial step. Small values of Manning's n generate small values of the friction head s_i, and thus small values of the total head, with error accumulating seaward. Since the Manning's n values
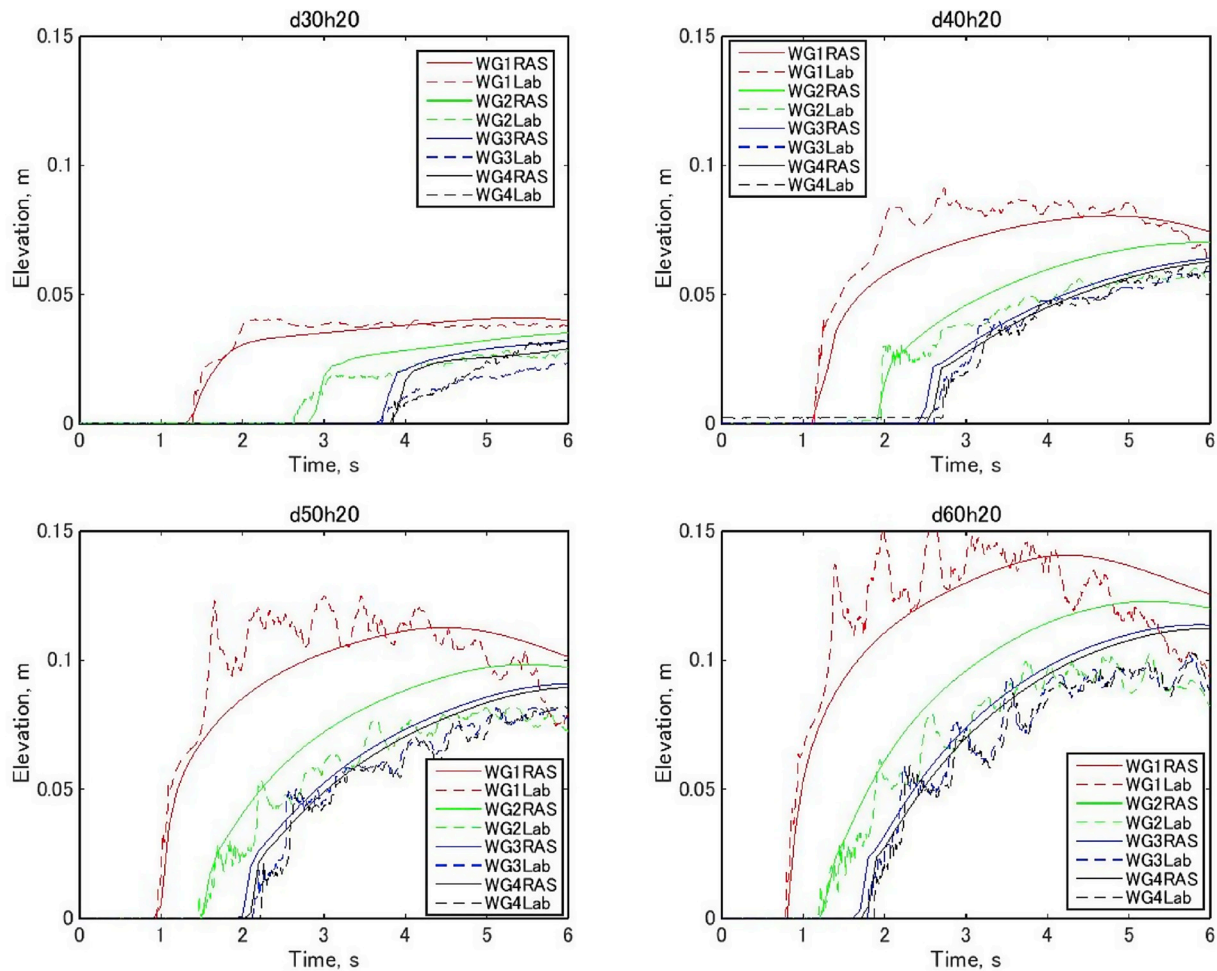
Fig. 12. Comparison of laboratory experiments (rough bed, no structure scenarios) and HEC-RAS time series (with $n = 0.03$ sm$^{-1/3}$) at wave gauges WG1 through WG4, for reservoir depths d of 30 cm, 40 cm, 50 cm, and 60 cm, released into a water depth in front of the reservoir h of 20 cm.

suggested by ASCE7 are much smaller than those suggested by Bricker et al. (2015) in urban and vegetated areas, the current EGL method appears non-conservative, requiring futher research into appropriate Manning's n values for tsunamis.

4. Discussion

The experiments detailed in this study, combined with the HEC-RAS computer simulations, and those performed by Glasbergen (2018) allowed the authors to obtain some insights into how accurately laboratory experiments can represent tsunami waves.

The roughness of the experiment bed used has a clear influence on the incoming tsunami front. The shape of the waves was different, with steeper fronts and lower Froude numbers for rough bed experiments. However, the different approaching flows did not noticeably change the observed response of the tested tsunami walls to the transient flow. The overtopping flow depth data collapsed onto the results of Esteban et al. (2017) for smooth walls, and provides further evidence that the equation of Esteban et al. (2017) might be applicable to real tsunamis. It also is further proof that the total head is a good parameter to describe the hydraulic response of the structure to the considered stationary/transient flow (while formally it is only valid for stationary flow). Herewith, the range of applicability of the formula has been increased to encompass a wider range of conditions.

The simulation of tsunamis in the laboratory is clearly difficult, as Froude numbers should match those of the real tsunamis. Glasbergen (2018) computed tsunami generation and runup for realistic ranges of

tsunami sources and coastal shapes, using the SWASH model (Zijlema et al., 2011). After calibration of the inundation depth and the runup height at the coast near the town of Yuriage, it was found that a Manning's n of 0.06 sm$^{-1/3}$ could reproduce the event well. Glasbergen (2018) then determined (slightly differently defined) Froude numbers for the bore fronts that resulted from these tsunamis, and compared them to the smooth bed tests (Esteban et al., 2017). For the smooth bed tests the bore-front Froude numbers at the location of the structure ranged from 1.45 to 2.69, while the bore-front Froude numbers of the simulations were much lower at that location (ranging from 0.65 to 1.14). However, the computed bore-front Froude numbers at the coast were 1.34–2.6, so essentially the inland bore-front Froude numbers (by Glasbergen, 2018) of the smooth bed tests match the Froude numbers of the simulations at the coast line. With the increased roughness the bore slows down and steepens, and this Froude number resembles the inland bore front-Froude number more closely.

A HEC-RAS simulation calibrated to the rough-bed laboratory experiments results in a Manning's n much higher than that suggested by ASCE7. The implications of this for disaster risk management are that the ASCE7 energy grade line (EGL) method is non-conservative. This is due to the friction loss in Equation (5) which, when added back into Equation (4) between the inundation limit and the shoreline, is smaller than the actual friction loss. However, for the USA this error may be mitigated since the original simulations used to generate the ASCE7 tsunami inundation maps also used Manning's n values that were too small, thereby resulting in conservative estimates for the limit of the inundation. A real danger is that the ASCE7 method may be applied by

non-US entities looking to use the EGL method with hazard maps that were not generated in the same way as the ASCE7 hazard maps. If the EGL method is applied with inundation maps based on historical data, for example, the resulting flow depths and speed estimated by the EGL method would be too small. This is particulary worrying given that the product of these two parameters largely determines mortality rates (with depth velocity products of over $1.2 \, \text{m}^2/\text{s}$ generally considered as the upper limit for pedestrians, Suga et al., 1995; Wright et al., 2010; Takagi et al., 2016).

The results of the present experiments thus emphasize the need to consider the incident bore velocity in the design of coastal protection structures. Video footage of the *2011 Tohoku Earthquake Tsunami* highlighted how in some areas the tsunami manifested itself as rapidly rising tide, in others as a slow bore, and yet in others as a rapidly advancing high velocity bore. This further emphasizes the need to start cataloguing tsunami waves into different types of waves, which should be clearly described and catalogued, rather than simply lumped together under the term "tsunami" (as in, efforts should be made to catalogue tsunami waves into different types, in the same way that breaking wind waves are differentiated into breaking, spilling and surging by the clearly defined Irribarren number, breaking solitary waves are classified by the solitary wave breaking criterion (Grilli et al., 1997), and breaking windwave groups are described by the normalized bed slope parameter (Battjes et al., 2004)). Glasbergen (2018), Roubos (2019), and Larsen and Fuhrman (2019a) present suggestions for such a quantitative classification of tsunami wave types. This difference in wave type will have implications for the design of coastal dykes, as under the current tsunami disaster management in Japan (which differentiates Level 1 and 2 events), coastal structures need to protect settlements against the expected inundation that could be brought about as a result of a 1 in 100 year tsunami (Level 1). The results thus indicate that this is not just a problem of how high to build the dyke, but that careful consideration needs to be given to the wave velocity and overtopping mechanism. While consideration of the failure mechanism is outside of the scope of this work, it is worth noting how lessons have been learnt as a consequence of the 2011 event, and that many new structures have improved leeward slope and toe protection (Kato et al., 2012; Mikami et al., 2014; Jayaratne et al., 2016).

5. Conclusions

The level of understanding on how to defend against tsunamis has greatly increased in the last 15 years, through observations in the aftermaths of the many events that have taken place in this period and important research efforts with laboratory experiments and computer simulations. Nevertheless, important challenges and gaps in knowledge still exist regarding how to accurately model these waves in the laboratory. In the present work the authors analysed how changes in bed roughness affect dam-break bores, and the resulting overtopping processes on three different structures, namely an "infinite" vertical wall, a dyke, and a low vertical wall.

The bores on rough floors had lower Froude numbers and steeper fronts. As a result, the range of applicability of the formula for overtopping flow depth by Esteban et al. (2017) has been increased to encompass this different type of rough-floor approach flow.

The results clearly corroborate the necessity of considering the energy present in the bore to determine whether a structure will be overtopped or not, which is a critical consideration considering how coastal structures in Japan should not be overtopped by a 1 in 100 tsunami event (Level 1). They also show the importance of clearly modelling the velocity and Froude number of a tsunami, and of conducting experiments using a realistic rough bed, for which a suitable Manning's n was 0.06 sm$^{-1/3}$ for both the experiments carried out (which correspond to a bed of cobbles at prototype scale) and for a SWASH model calibrated by Glasbergen (2018) for the tsunami inundation of Yuriage in 2011. Otherwise, the use of a smooth bed in

tsunami experiments might result in waves that do not accurately reproduce the real phenomena observed in nature (though the present experiments also indicate that they would represent conservative estimates, as compared to rough beds).

References

ASCE, 2016. ASCE 7 Standard, Minimum Design Loads and Associated Criteria for Buildings and Other Structures ASCE7-16. Chapter 6 – Tsunami Loads and Effects. American Society of Civil Engineers.

Battjes, J.A., Bakkenes, H.J., Janssen, T.T., Van Dongeren, A.R., 2004. Shoaling of sub-harmonic gravity waves. J. Geophys. Res.: Oceans 109 (C2).

Bricker, J.D., Inagaki, S., Monismith, S.G., 2005. Bed drag coefficient variability under wind waves in a tidal estuary. J. Hydraul. Eng. 131 (6), 497–508.

Bricker, J.D., Francis, M., Nakayama, A., 2012. Scour depths near coastal structures due to the 2011 Tohoku Tsunami. J. Hydraul. Res. 50 (6), 637–641.

Bricker, J.D., Gibson, S., Takagi, H., Imamura, F., 2015. On the need for larger Manning's roughness coefficients in depth-integrated tsunami inundation models. Coast Eng. J. 57 (02) 1550005.

Bricker, J.D., Schwanghart, W., Adhikari, B.R., Moriguchi, S., Roeber, V., Giri, S., 2017. Performance of models for flash flood warning and hazard assessment: the 2015 Kali Gandaki landslide dam breach in Nepal. Mt. Res. Dev. 37 (1), 5–16.

Bruner, G.W., 2016. HEC-RAS River Analysis System Hydraulic Reference Manual CPD-69. US Army Corps of Engineers, Hydraulic Engineering Centre, pp. 8–12.

Chanson, H., 2006. Analytical solutions of laminar and turbulent dam break wave. In: In: Ferreira, R.M.L., Alves, E.C.T.L., Leal, J.G.A.B., Cardoso, A.H. (Eds.), Proc. Int. Conf. Fluvial Hydraulics River Flow 2006, vol. 1. Taylor & Francis Groupe, London, pp. 465–474 ISBN:0-415-40815-6.

Chock, G., 2015. The ASCE7 tsunami loads and effects design standard for the U.S. In: Esteban, M., Takagi, H., Shibayama, T. (Eds.), Handbook of Coastal Disaster Mitigation for Engineers and Planners. Butterworth-Heinemann (Elsevier), Oxford, UK.

Chow, V.T., 1959. Open Channel Hydraulics. McGraw-Hill Book Company, New York, pp. 680p.

Cyranoski, D., 2012. After the deluge: Japan is rebuilding its coastal cities to protect people from the biggest tsunamis. Nature 483, 141–143.

Dressler, R.F., 1954. Comparison of theories and experiments for hydraulic dam-break wave. Int. Assoc. Sci. Pubs 38 (3), 319–328.

Esteban, M., Danh Thao, N., Takagi, H., Shibayama, T., 2009. Pressure exerted by a solitary wave on the rubble mound foundation of an armoured caisson breakwater. In: 19th International Offshore and Polar Engineering Conference, Osaka.

Esteban, M., Glasbergen, T., Takabatake, T., Hofland, B., Nishizaki, S., Nishida, Y., Stolle, J., Nistor, I., Bricker, J., Takagi, H., Shibayama, T., 2017. Overtopping of coastal structures by tsunami waves. Geosciences 7 (4), 121. https://doi.org/10.3390/geosciences7040121.

Esteban, M., Morikubo, I., Shibayama, T., Aranguiz Muñoz, R., Mikami, T., Danh Thao, N., Ohira, K., Ohtani, A., 2012a. Stability of rubble mound breakwaters against solitary waves". In: Proc. of 33th Int. Cdonf. on Coastal Engineering, Santander, Spain..

Esteban, M., Takagi, H., Shibayama, T., 2012b. Modified goda formula to simulate sliding of composite caisson breakwater. Coast Eng. J. 54 (04). https://doi.org/10.1142/S0578563412500222.

Esteban, M., Jayaratne, R., Mikami, T., Morikubo, I., Shibayama, T., Danh Thao, N., Ohira, K., Ohtani, A., Mizuno, Y., Kinoshita, M., Matsuba, S., 2014. Stability of breakwater armour units against tsunami attack. J. Waterw. Port, Coast. Ocean Eng. 140, 188–198.

Esteban, M., Onuki, M., Ikeda, I., Akiyama, T., 2015. In: Esteban, M., Takagi, H., Shibayama, T. (Eds.), "Reconstruction Following the 2011 Tohoku Earthquake Tsunami: Case Study of Otsuchi Town in Iwate Prefecture, Japan" in Handbook of Coastal Disaster Mitigation for Engineers and Planners. Butterworth-Heinemann (Elsevier), Oxford, UK.

Estrade, J., Martinot, A., 1964. Ecoulment consecutif a la suppression dun barrage dans un canal horizontal de section rectangulaire. Comptes Rendus Hebdomadaires des Seances de L'Acadmie Des Sciences 259 (25), 4502 (in french).

EERI, Earthquake Engineering Research Institute Special Earthquake Report, 2011. Learning from Earthquakes: the Tohoku, Japan, Tsunami of March 11, 2011. Effects on Structures, pp. 14pp.

Goseberg, N., Wurpts, A., Schlurmann, T., 2013. Laboratory-scale generation of tsunami and long waves. Coast. Eng. 79, 57tal.

Glasbergen, T., 2018. Parameters of incoming tsunami bores for the design of coastal defence structures. Master Thesis. TUDelft. https://repository.tudelft.nl/islandora/object/uuid%3Aad229966-5403-432d-9a13-84a9e7fdb5bc?collection=education.

Grilli, S.T., Svendsen, I.A., Subramanya, R., 1997. Breaking criterion and characteristics for solitary waves on slopes. J. Waterw. Port, Coast. Ocean Eng. 123 (3), 102–112.

Hanzawa, M., Matsumoto, A., Tanaka, H., 2012. Stability of wave-dissipating concrete blocks of detached breakwaters against tsunami. In: Proc. of the 33rd Int. Conference on Coastal Engineering [ICCE].

Hunt-Raby, A., Borthwick, A.G.L., Stansby, P.K., Taylor, P.H., 2011. Experimental measurement of focused wave group and solitary wave overtopping. J. Hydraul. Res. 49 (4), 450–464.

Ikeno, M., Mori, N., Tanaka, H., 2001. Experimental study on tsunami force and impulsive force by a drifter under breaking bore like tsunamis. Proc. Coast. Eng., JSCE 48, 846–850.

Ikeno, M., Tanaka, H., 2003. Experimental study on impulse force of drift body and tsunami running up to land. Proc. Coast. Eng., JSCE 50, 721–725.

Iwate Prefecture Tsunami Disaster Prevention Technical Committee, 2013. Reference materials #1. Available at: https://www.pref.iwate.jp/area/shingikai/kendo/tsunami/023437.html, Accessed date: 8 April 2019.

Jayaratne, M.P.R., Premaratne, B., Adewale, A., Mikami, T., Matsuba, S., Shibayama, T., Esteban, M., Nistor, I., 2016. Failure mechanisms and local scour at coastal structures induced by tsunami. Coast Eng. J. 58, 04.

Jonkman, S.N., Penning-Rowsell, E., 2008. Human instability in flood flows. J. Am. Water Resour. Assoc. 44 (5), 1208–1218.

Kato, F., Suwa, Y., Watanabe, K., Hatogai, S., 2012. Mechanism of coastal dike failure induced by the great east Japan Earthquake tsunami. In: Proc. Of 33nd Int. Conf. on Coastal Engineering Santander, Spain.

Kriebel, D.L., Lynett, P.J., Cox, D.T., Petroff, C.M., Robertson, I.N., Chock, G.Y., 2017. Energy method for approximating overland tsunami flows. J. Waterw. Port, Coast. Ocean Eng. 143 (5) 04017014.

Latcharote, P., Suppasri, A., Hasegawa, N., Takagi, H., Imamura, F., 2016. Effect of breakwaters on reduction of fatality ratio during the 2011 great east Japan Earthquake and tsunami. J. Jpn Soc. Civil Eng., Ser. B2 (Coast. Eng.) 72 (2), 1591–1596.

Larsen, B.E., Fuhrman, D.R., 2019a. Full-scale CFD simulation of tsunamis. Part 1: model validation and run-up. Coast. Eng. 151, 22–41.

Larsen, B.E., Fuhrman, D.R., 2019b. Full-scale CFD simulation of tsunamis. Part 2: boundary layers and bed shear stresses. Coast. Eng. 151, 42–57.

Limerinos, J.T., 1970. Manning Coefficient from Measured Bed Roughness in Natural Channels. US Geological Survey Water Supply Paper 1898-B.

Madsen, P.A., Furhman, D.R., Schaffer, H.A., 2008. On the solitary wave paradigm for tsunamis. J. Geophys. Res. 113, C12012.

Matsutomi, H., Shuto, N., Imamura, F., Takahashi, T., 2001. Filed survey of the 1996 irian jaya Earthquake tsunami in biak island. Nat. Hazards 24 (3), 199–212.

Mikami, T., Shibayama, T., Esteban, M., Matsumaru, R., 2012. Field survey of the 2011 Tohoku Earthquake and tsunami in miyagi and fukushima prefectures. Coast Eng. J. 54 (1), 1–26.

Mikami, T., Matsuba, S., Shibayama, T., 2014. Flow geometry of overflowing tsunamis around coastal dykes. Coastal Eng. Proc. https://journals.tdl.org/icce/index.php/icce/article/view/7615/pdf_839, Accessed date: 1 June 2016.

Mizutani, S., Imamura, F., 2000. Hydraulic experimental study on wave force of a bore acting on a structure. Proc. Coast. Eng., JSCE 47, 946–950.

Mori, N., Takahashi, T., et al., 2012. The 2011 Tohoku Earthquake tsunami joint survey group [2012] nationwide survey of the 2011 Tohoku Earthquake tsunami. Coast Eng. J. 54 (1), 1–27.

Nandasena, N.A.K., Sasaki, Y., Tanaka, N., 2012. Modelling field observations of the 2011 Great East Japan tsunami: efficacy of artificial and natural structures on tsunami mitigation. Coast Eng. 67, 1–13.

Nateghi, R., Bricker, J.D., Guikema, S.D., Bessho, A., 2016. Statistical analysis of the effectiveness of seawalls and coastal forests in mitigating tsunami impacts in Iwate and Miyagi prefectures. PLoS One 11 (8), e0158375.

Omira, R., Baptista, M.A., Leone, F., Matias, L., Mellas, S., Zourarah, B., Miranda, J.M., Carrilho, F., Cherel, J.P., 2013. Performance of coastal sea-defence infrastructure at El Jadida (Marocco) against tsunami threat: lessons learned from the Japanese 11 March tsunami. Nat. Hazards Earth Syst. Sci. 13, 1779–1794.

Okumura, N., Jonkman, S.N., Esteban, M., Hofland, B., Shibayama, T., 2017. A method for tsunami risk assessment - a case study for Kamakura, Japan. Nat. Hazards. https://doi.org/10.1007/s11069-017-2928-x.

Ranghieri, F., Ishiwatari, M., 2014. Megadisasters. Lessons from the great east Japan Earthquake. Available at. https://openknowledge.worldbank.org/bitstream/handle/10986/.../9781464801532.pdf, Accessed date: 11 July 2016.

Roubos, J., 2019. Prediction of the characteristics of a tsunami wave near the Tohoku coastline. Master thesis. TU Delft. https://repository.tudelft.nl/islandora/object/uuid%3A421cd6b8-fd31-424a-aa9b-529dc17018eb?collection=education.

San Carlos-Arce, R., Onuki, M., Esteban, M., Shibayama, T., 2017. Risk awareness and intended tsunami evacuation behaviour of international tourists in Kamakura city, Japan. Int. J. Disaster Risk Reduct. 23, 178–192.

Sakakiyama, T., 2012. Stability of armour units of rubble mound breakwater against tsunamis. In: Proc. Of 32nd Int. Conf. on Coastal Engineering, Santander, Spain.

Shibayama, T., Esteban, M., Nistor, I., Takagi, H., Danh Thao, N., Matsumaru, R., Mikami, T., Aranguiz, R., Jayaratne, R., Ohira, K., 2013. Classification of tsunami and evacuation areas. J. Nat. Hazards 67 (2), 365–386.

Stansby, P., Xu, R., Rogers, B.D., Hunt-Raby, A., Borthwick, A.G.L., Taylor, P.H., 2008. Modelling overtopping of a sea defence by shallow-water Boussinesq, VOF and SPH methods. In: Proc. Of Flood Risk Assessment Conference, Oxford.

Stolle, J., Stolle, J., Krautwald, C., Robertson, I., Achiari, H., Mikami, T., Nakamura, R., Takabatake, T., Nishida, Y., Shibayama, T., Esteban, M., Nistor, I., Goseberg, N., 2019. Engineering lessons from the 18 september 2018 Indonesian tsunami: debris loading. Can. Hydraul. J (provisionally accepted).

Suga, K., Uesaka, T., Yoshida, T., Hamaguchi, H., Chen, Z., 1995. Preliminary study on feasible safe evacuation in flood disaster. Proc. Hydraul. Eng. JSCE 39, 879–882.

Supparsi, A., Koshimura, S., Imai, K., Mas, E., Gokon, H., Muhari, A., Imamura, F., 2012. Damage characteristic and field survey of the 2011 great east Japan tsunami in miyagi prefecture. Coast Eng. J. 54, 1250005.

Takagi, H., Bricker, J., 2014. Assessment of the effectiveness of general breakwaters in reducing tsunami inundation in Ishinomaki. Coast Eng. J. 56 (4).

Tanimoto, L., Tsuruya, K., Nakano, S., 1984. Tsunami force of nihonkai-chubu Earthquake in 1983 and cause of revetment damage. In: Proceeding of the 31st Japanese Conference on Coastal Engineering. JSCE.

Takabatake, T., Shibayama, T., Esteban, M., Ishii, H., Hamano, G., 2017. Simulated tsunami evacuation behaviour of local residents and visitors in kamakura, Japan. Int. J. Disaster Risk Reduct. 23, 1–14.

Takabatake, T., Shibayama, T., Esteban, M., Ishii, H., 2018. Advanced casualty estimation based on tsunami evacuation intended behavior: case study at Yuigahama Beach, Kamakura, Japan. Nat. Hazards 1–26. https://doi.org/10.1007/s11069-018-3277-0].

Takagi, H., Li, S., de Leon, M., Esteban, M., Mikami, T., Matsumaru, R., Shibayama, T., Nakamura, R., 2016. Storm surge and evacuation in urban areas during the peak of a storm. Coast Eng. 108, 1–9. https://doi.org/10.1016/j.coastaleng.2015.11.002.

Tomita, T., Yeom, G-S., Ayugai, M., Niwa, T., 2012. Breakwater effects on tsunami inundation reduction in the 2011 off the pacific coast of Tohoku Earthquake. J. Jpn Soc. Civil Eng., series B2 (Coast. Eng.) 68 (2) I_156-60.

Tonkin, S.P., Francis, M., Bricker, J.D., 2014. Limits on coastal scour depths due to tsunami. In: International Efforts in Lifeline Earthquake Engineering. ASCE, pp. 671–678.

Williams, I.A., Fuhrman, D.R., 2016. Numerical simulation of tsunami-scale wave boundary layers. Coast. Eng. 110, 17–31.

Wright, K., Doody, B.J., Becker, J., McClure, J., 2010. Pedestrian and Motorist Flood Safety Study: A Review of Behaviours in And Around Floodwater and Strategies to Enhance Appropriate Behaviour. GNS Science Report 2010/51. pp. 91.

Yamao, S., Esteban, M., Yun, N.Y., Mikami, T., Shibayama, T., 2015. In: Esteban, M., Takagi, H., Shibayama, T. (Eds.), "Estimation of the Current Risk to Human Damage Life Posed by Future Tsunamis in Japan" in Handbook of Coastal Disaster Mitigation for Engineers and Planners. Butterworth-Heinemann (Elsevier), Oxford, UK.

Zijlema, M., Stelling, G., Smit, P., 2011. SWASH: an operational public domain code for simulating wave fields and rapidly varied flows in coastal waters. Coast. Eng. 58, 992–1012.